arXiv:nucl-th/0410082v1 19 Oct 2004

Self-consistent Green's function calculations of ^{16}O at small missing energies

C. Barbieri†§ and W. H. Dickhoff‡

† TRIUMF, 4004 Wesbrook Mall, Vancouver, British Columbia, Canada V6T 2A3

‡ Department of Physics, Washington University, St.Louis, Missouri 63130, USA

Abstract. Calculations of the one-hole spectral function of ^{16}O for small missing energies are reviewed. The self-consistent Green's function approach is employed together with the Faddeev equations technique in order to study the coupling of both particle-particle and particle-hole phonons to the single-particle motion. The results indicate that the characteristics of hole fragmentation are related to the low-lying states of ^{16}O and an improvement of the description of this spectrum, beyond the random phase approximation, is required to understand the experimental strength distribution. A first calculation in this direction that accounts for two-phonon states is discussed.

§ Email: barbieri@triumf.ca

1. Introduction

Recent advances in nuclear theory have generated accurate predictions for the spectrum of most p shell nuclei (see, for instance, Refs. [1, 2]). At the same time, other techniques are becoming available to describe larger systems and to account for the effects of the continuum [3, 4]. For medium and heavy systems, relevant information regarding correlations has been obtained by studying the nuclear spectral function. This was mainly done by means of variational calculations [5] and the self-consistent Green's function (SCGF) [6] approaches.

Once a given nuclear Hamiltonian is chosen, quantities such as the spectroscopic factors are defined uniquely in term of the exact solutions of the many-body problem. Thus, their knowledge gives direct information on the correlations induced by that specific nuclear force. Experimentally, $(e, e'p)$ reactions have provided results for knock out from orbits both close to [7, 8] and far from [9] the Fermi energy. Although a consistent calculation (based on the same Hamiltonian) of the initial and final states has so far been possible only for specific cases [10], several analyses [11, 12, 13, 7] suggest that the experimental cross section can be described by standard phenomenological realistic interactions. This leads to fragments at small missing energies that have spectroscopic factors of about 60-70% [7]. Moreover, recent measurements of the spectral function at high missing energies and momenta [14] appear to be consistent with the tail due to the short-range and tensor correlations (SRC) that are induced by nuclear forces having a repulsive core. Whether (and how) softer NN interactions can describe these measurements is an open (and interesting) question.

For the case of ^{16}O, there still exists a substantial disagreement between the quenching of spectroscopic factors extracted from the experiment [8, 10, 12] and theory [15, 16, 17]. The latter results suggest that the reasons for this discrepancy should be looked for in the effects of long-range correlations (LRC) and in particular in the couplings of single-particle (sp) motion to low-energy collective excitations. In this contribution we report about the work done along this line in Refs. [17, 18] in order to tackle the above issues for ^{16}O. Sec. 2 describes the SCGF and Faddeev formalism employed to couple sp and collective phonons [19]. The results for the hole spectral function are discussed in Sec. 3. These calculations show that a proper description of the experimental spectral strength requires an improvement of the spectrum which goes beyond the random phase approximation (RPA). A first step in this direction that includes the propagation two-phonon states is reported in Sec. 4.

2. Faddeev approach for the single-particle Green's function

We consider the calculation of the sp Green's function

$$g_{\alpha\beta}(\omega) \;=\; \sum_n \frac{(\mathcal{X}^n_\alpha)^* \;\mathcal{X}^n_\beta}{\omega - \varepsilon^+_n + i\eta} \;+\; \sum_k \frac{\mathcal{Y}^k_\alpha \left(\mathcal{Y}^k_\beta\right)^*}{\omega - \varepsilon^-_k - i\eta}\,, \tag{1}$$

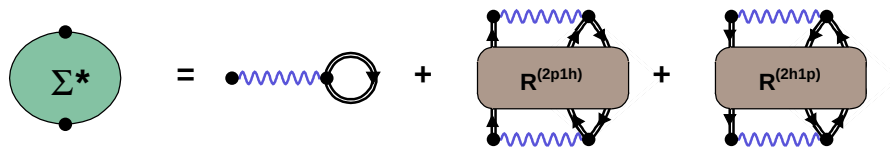

Figure 1. Diagrams contributing to the irreducible self-energy Σ^*. The double lines represent a dressed propagator and the wavy lines correspond to a G-matrix (that is used in this work as an effective interaction). The first term is the Brueckner-Hartree-Fock potential while the others represent the 2p1h/2h1p or higher contributions that are approximated through the Faddeev TDA/RPA equations.

from which both the one-hole and one-particle spectral functions, for the removal and addition of a nucleon, can be extracted. In Eq. (1), $\mathcal{X}_\alpha^n = \langle \Psi_n^{A+1} | c_\alpha^\dagger | \Psi_0^A \rangle$ ($\mathcal{Y}_\alpha^k = \langle \Psi_k^{A-1} | c_\alpha | \Psi_0^A \rangle$) are the spectroscopic amplitudes for the excited states of a system with $A+1$ ($A-1$) particles and the poles $\varepsilon_n^+ = E_n^{A+1} - E_0^A$ ($\varepsilon_k^- = E_0^A - E_k^{A-1}$) correspond to the excitation energies with respect to the A-body ground state. The one-body Green's function can be computed by solving the Dyson equation

$$g_{\alpha\beta}(\omega) = g^0_{\alpha\beta}(\omega) \; + \; \sum_{\gamma\delta} g^0_{\alpha\gamma}(\omega) \Sigma^*_{\gamma\delta}(\omega) g_{\delta\beta}(\omega) \quad , \tag{2}$$

where the irreducible self-energy $\Sigma^*_{\gamma\delta}(\omega)$ acts as an effective, energy-dependent, potential. The latter can be expanded in a Feynman-Dyson series [20, 21] in terms the exact propagator $g_{\alpha\beta}(\omega)$, which itself is a solution of Eq. (2). In this expansion, $\Sigma^*_{\gamma\delta}(\omega)$ can be represented as shown in Fig. 1 by the sum of a dressed Hartree-Fock potential and terms that describe the coupling between the sp motion and more complex excitations [6]. It is at the level of the 2p1h/2h1p propagator, $R(\omega)$, that the correlations involving interactions between different collective modes have to be included.

The SCGF approach can be initiated by solving the self-energy and the Dyson Eq. (2) in terms of an unperturbed propagator $g^0_{\alpha\beta}(\omega)$. The (dressed) solution $g_{\alpha\beta}(\omega)$ is then used to evaluate an improved self-energy, which then contains the effects of fragmentation. The whole procedure is iterated until self-consistency is reached. Baym and Kadanoff showed that a self-consistent solution of the above equation guarantees the fulfillment of the principal conservation laws [22].

2.1. Faddeev approach to the self-energy

In the following we are interested in describing the coupling of sp motion to ph and pp(hh) collective excitations of the system. All the relevant information regarding the latters are included in the Lehmann representations of the polarization propagator

$$\Pi_{\alpha\beta,\gamma\delta}(\omega) = \sum_{n\neq 0} \frac{\langle \Psi_0^A | c_\beta^\dagger c_\alpha | \Psi_n^A \rangle \; \langle \Psi_n^A | c_\gamma^\dagger c_\delta | \Psi_0^A \rangle}{\omega - (E_n^A - E_0^A) + i\eta}$$

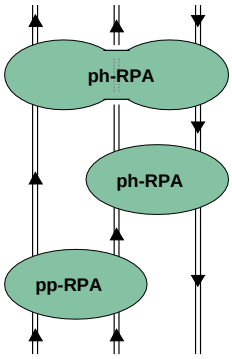

Figure 2. Example of a diagram appearing in the all-orders summation generated by the set of Faddeev equations.

$$- \sum_{n\neq 0} \frac{\langle \Psi_0^A | c_\gamma^\dagger c_\delta | \Psi_n^A \rangle \, \langle \Psi_n^A | c_\beta^\dagger c_\alpha | \Psi_0^A \rangle}{\omega - (E_0^A - E_n^A) - i\eta} \, , \tag{3}$$

and the two-particle propagator

$$\begin{aligned} g^{II}_{\alpha\beta,\gamma\delta}(\omega) = & \sum_n \frac{\langle \Psi_0^A | c_\beta c_\alpha | \Psi_n^{A+2} \rangle \, \langle \Psi_n^{A+2} | c_\gamma^\dagger c_\delta^\dagger | \Psi_0^A \rangle}{\omega - (E_n^{A+2} - E_0^A) + i\eta} \\ & - \sum_k \frac{\langle \Psi_0^A | c_\gamma^\dagger c_\delta^\dagger | \Psi_k^{A-2} \rangle \, \langle \Psi_k^{A-2} | c_\beta c_\alpha | \Psi_0^A \rangle}{\omega - \left(E_0^A - E_k^{A-2}\right) - i\eta} \, . \end{aligned} \tag{4}$$

which describe the excited states of the systems with A and $A \pm 2$ particles, respectively. In general, Eqs. (3) and (4) are the exact solutions of their respective Bethe-Salpeter equations (BSE). In the calculation of Sec. 3, these have been approximated by solving the dressed Tamm-Dancoff/RPA (DTDA/DRPA) equations [23, 24], which account for the effects of the strength distribution of the particle and hole fragments. The inclusion of correlations beyond RPA is considered in Sec. 4.

The ph (3) and pp(hh) (4) propagators are inserted in the nuclear self-energy by solving a set of Faddeev equations [25] for the 2p1h and 2h1p propagators of Fig. 1. The details of this approach are given in Ref. [19]. For the present discussion it is sufficient to note that the motion of three-quasiparticle excitations is approached in the same way it is normally done for the three-body problem. Collective excitations are coupled to sp propagators generating an infinite series of diagrams, including the one shown in Fig. 2. This allows to account completely for Pauli correlations at the 2p1h/2h1p level.

3. Results for the single-particle spectral function of ^{16}O

In the calculations described below, the Dyson equation was solved in a model space consisting of harmonic oscillator sp states. An oscillator parameter $b = 1.76$ fm was chosen (corresponding to $\hbar\omega = 13.4$ MeV) and all the first four major shells (from $1s$ to $2p1f$) plus the $1g_{9/2}$ where included. The results of Refs. [24, 18], suggest that this model space is large enough to properly account for the low-energy collective states if fragmentaion is accounted for. Inside the model space, a Brueckner G-matrix [26] derived from the Bonn-C potential [27] was used as an effective interaction. The

Shell	TDA	RPA	1st itr.	2nd itr.	3rd itr.	4th itr.
$Z_{p_{1/2}}$	0.775	0.745	0.775	0.777	0.774	0.776
$Z_{p_{3/2}}$	0.766	0.725	0.725	0.727	0.722	0.724
			0.015	0.027	0.026	0.026

Table 1. Hole spectroscopic factors (Z_α) for knockout of a $\ell = 1$ proton from ^{16}O. The columns 'TDA' and 'RPA' refer to the initial undressed calculations, while the remaining colums resulted from the first four iterations of the DRPA equations. Note that the iterated resulted were obtained by constraining the lowest 0^+ solution for ^{16}O at its experimantal value, which is at the origin of the fragmentation of the $p_{3/2}$ peak.

short-range core of this NN interaction induce an additional 10 % reduction in the spectroscopic factors [6], which is accounted for in the solution of the Dyson equation through the energy dependence of the G-matrix.

3.1. Effects of RPA correlations and fragmentation

For an unperturbed initial propagator the TDA calculation is equivalent to the one of Ref. [16] and yields spectroscopic factors equal to 0.775 and 0.766 for the main $p_{1/2}$ and $p_{3/2}$ qhasihole peaks, respectively. These results are reported in Table 1. The introduction of RPA correlations reduces these values and brings them down to 0.745 and 0.725, respectively. This shows that collectivity beyond the TDA level is relevant to explain the quenching of spectroscopic factors. We note that due to center-of-mass effects, the above quantities might need to be increased by about 7% before they are compared with the experiment [28].

The RPA results were then iterated a few times to study the effects of fragmentation. Since only the low-energy excitations are of interest here, it is sufficient to keep track only of the largets fragments that appear —close to the Fermi energy— in the (dressed) sp propagator, Eq. (1), while the residual strength is collected in a effective pole [29, 17]. Only a few iterations were required to reach convergence. The effect of including fragmentation in the construction of the RPA phonons is to increase the strength of the main hole peaks. The $p_{1/2}$ strength increases from the 0.745, obtained with the undressed input, to 0.776. Analogously the total strength in the $p_{3/2}$ peak rises to 0.750. This behavior is due to the competing effect of the redistribution of the strength, which tends to screen the nuclear interaction.

The converged distribution of one-hole strength is shown in the mid panels of Fig. 3, where it is compared to the experiment (top panels). The latter is characterized by additional small fragments close to the Fermi energy, some of which will be discussed in Sec. 3.2. We note that similar results are obtained for the particle strength, including large peaks near the Fermi level and a fragmented distribution at larger energies. This self-energy at positive energies has been employed recently in studying low energy

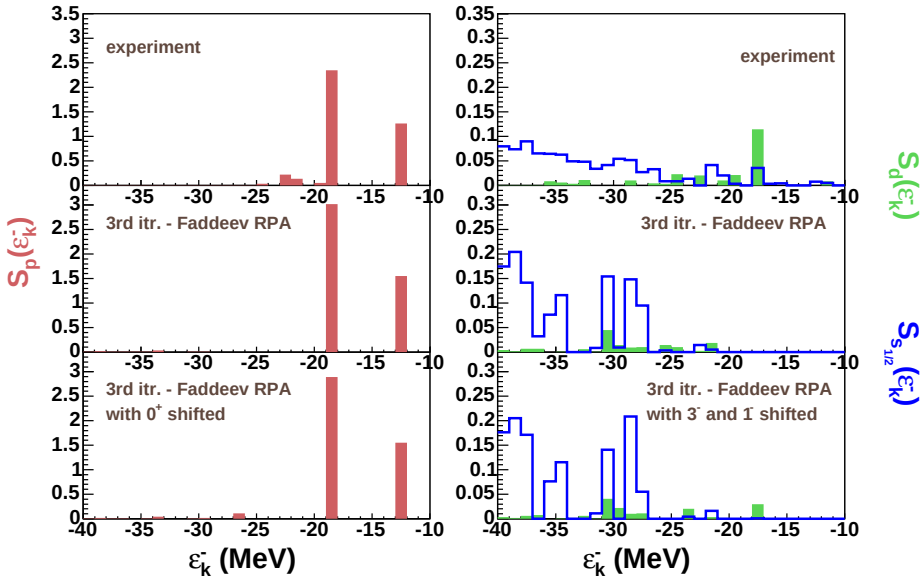

Figure 3. One-proton removal strength as a function of the hole sp energy $\varepsilon_k^- = E_0^A - E_k^{A-1}$ for ^{16}O for angular momentum $\ell = 1$ (left) and $\ell = 0, 2$ (right). For the positive parity states, the solid bars correspond to results for $d_{5/2}$ and $d_{3/2}$ orbitals, while the thick lines refer to $s_{1/2}$. The top panels show the experimental values taken from [8]. The mid panels give the theoretical results for the self-consitent spectral function. The bottom panels show the results obtained by repeating the 3$^{\rm rd}$ iteration with a modified ph-DRPA spectrum, in which the lowest eigenstates have been shifted to the corresponding experimental values.

proton-nucleus scattering [30].

3.2. Role of the lowest excited states in ^{16}O

A deeper insight into the mechanisms that generate the fragmentation pattern can be gained by investigating directly the connection between the spectral function and some specific collective states. To clarify this point we repeated the above calculations of the sp propagator by shifting, at each iteration, the solution for the lowest 0^+ excitation in ^{16}O to its experimental energy. The difference with respect to the preceding results is the appearance of a second smaller $p_{3/2}$ fragment at -26.3 MeV, which might be interpreted as one of the fragments seen experimentally at slightly higher energy. This solution arises in the first two iterations and converges to a spectroscopic factor of 2.6%, as seen in Table 1. The associated p hole spectral function is shown in the lower-left panel of Fig. 3. This result can be interpreted by considering the $p_{3/2}$ fragments as generated by holes in the ground state and an excited 0^+ level of the ^{16}O core. If the two levels are close enough in energy, the two configurations mix together with the result of fragmenting the strength over more than one peak.

The other two low-lying states of ^{16}O that may be of some relevance are the isoscalar 1^- and 3^-, which are reproduced by RPA type calculations at $\sim$3 MeV above the

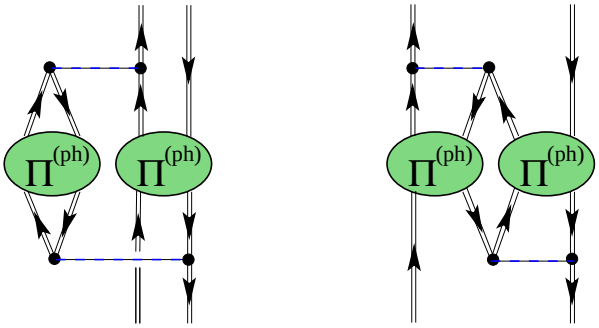

Figure 4. Examples of contributions involving the coupling of two independent ph phonons. All the diagrams of this type, obtained by considering all the possible couplings to a ph state, are included in the BSE kernel by the two-phonon ERPA equations of Ref. [18].

experiment (see Fig. 5 below). The lower-right panel of Fig. 3 shows the results for the even parity spectral functions that are obtained when both the 3^- and the 1^- ph-DRPA solutions are shifted to match their experimental values. In this case, a $d_{5/2}$ hole peak is obtained at a missing energy of -17.7 MeV, in agreement with experiment.

4. Two-photon contributions to the spectrum of ^{16}O

The above results suggest that an improvement of the solution for the spectral strength would require a better description of the excitation spectrum. One important problem of (D)RPA is the appearance of at most one collective phonon for a given J^π, T combination while several low-lying isoscalar 0^+ and 2^+ excited states are observed at low energy in ^{16}O, as well as additional 3^- and 1^- states. A good description of the spectrum of ^{16}O was obtained in Ref. [31] by coupling up to four different phonons with negative parity (3^- and 1^-). However, the self-consistent role of coupling positive parity states and the dressing of sp propagators were not investigated. These effects allow for the partial inclusion of configurations beyond 2p2h already at the two-phonon level. Moreover, the inclusion of two-phonon excitations represent the first correction to the DRPA equation generated by the Baym-Kadanoff formalism [32]. These conisist of diagrams like the ones of Fig. 4 that have been included in to the kernel of the BSE. The relative formalism has been presented in Ref. [18], where it is referred to as "two-phonon extended RPA (ERPA)". In this work the ph-DRPA equation has been solved first, using the self-consistent sp propagator derived in Sec. 3. The lowest DRPA solutions for both the 0^+, 3^- and 1^- channels were shifted down to their relative experimental energies and then they were employed to generate the two-phonon contributions for the ERPA calculation.

We note that the solution for the first isoscalar 0^+ state in DRPA is found much higher in energy at $\sim$17 MeV and it has a sharp ph character. Therefore it cannot be identified with the experimental 0_2^+ state, whose shell model structure is dominated by $4\hbar\omega$ configurations [33]. On the other hand inelastic electron scattering experiments clearly excite this state [34]. The one-body response is described by the polarization propagator, Eq. (3), and therefore the total experimental strength must be represented by Z_{n_π}, Eq. (5). This indicates a strong coupling to ph configurations (where "ph" actually means "quasiparticle-quasihole", with bare np-nh configurations implicitly

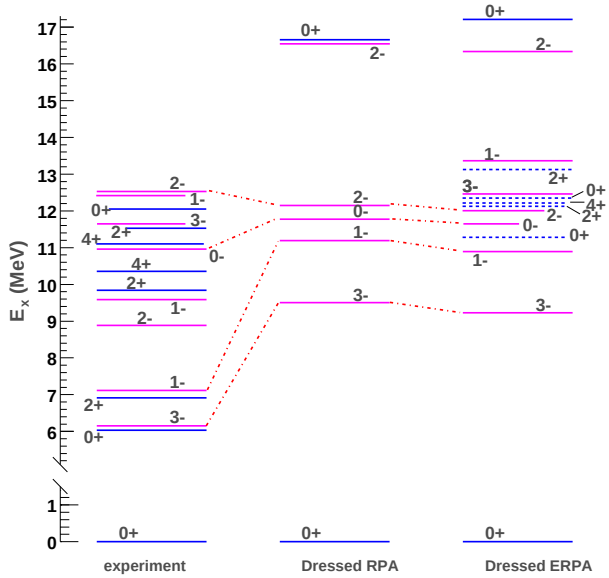

Figure 5. Results for the DRPA and the two-phonon ERPA spectra of ^{16}O obtained using the dressed input propagator computed in Sec. 3, middle and right plots, respectively. In solving the ERPA equation, the lowest 3^-, 1^- and 0^+ levels of the DRPA propagator where shifted to their experimental energies. All other DRPA solutions were left unchanged. The ERPA solutions indicated by dashed lines are those with a predominant two-phonon chatacter. The experimental spectrum is shown on the left.

included by the dressing of the sp propagator). On the basis of this similarity —and as long as one keeps in mind its limitations— it still appears interesting to shift the lowest 0^+ ph-DRPA solution down in energy and investigate how it mixes with other configurations.

The ERPA spectrum obtained for ^{16}O is displayed in Fig. 5 and Table 2 together with the total ph strength Z_{n_π} of each state,

$$Z_{n_\pi} \;=\; \sum_{\alpha\beta} \left|\langle \Psi^A_{n_\pi} | c^\dagger_\alpha c_\beta | \Psi^A_0 \rangle\right|^2 \quad , \tag{5}$$

and the relative occupations of ph and two-phonon admixtures in its wave function. An isoscalar 0^+ state with a predominant ph character is still found at $\sim$17 MeV, as in DRPA, but it is now characterized by a partial contribution from two-phonon configurations. Table 2 shows that this mixing results in a lower solution at $\sim$11 MeV, which is predominately a two-phonon state. In both cases the relevant configuration comes from the coupling of two 0^+ phonons themselves. Of course higher configurations, including three- and four-phonon states, should be included to reach a complete understanding of the 0^+ spectrum. A study of these will be pursued in the future.

The low-lying 3^- and 1^- states are only slightly affected by two-phonon contributions and remain substantially above the experimental energy at 9.23 and 10.90 MeV. However, the coupling of these to the 0^+_2 level reproduce the second excited states for the same angular momentum and parity. The two-phonon ERPA approach also generates a triplet of states at about 12 MeV with quantum numbers 0^+, 2^+ and 4^+. The solutions for this triplet are almost exclusively made of $3^- \otimes 3^-$ configurations and therefore have a 2p2h character. A similar triplet is found experimentally at 12.05, 11.52 and 11.10 MeV, which correspond to twice the experimental energy of the first 3^- phonon.

$T=0$	dressed/DRPA		dressed/ERPA				$(0_2^+)^2$	$(3_1^-)^2$	$(0_2^+, 3_1^-)$	$(0_2^+, 1_1^-)$
J^π	ε_n^π	Z_{n_π}	ε_n^π	Z_{n_π}	$ph(\%)$	$2\Pi(\%)$	(%)	(%)	(%)	(%)
1^-			13.37	0.148	21	79				79
3^-			12.35	0.113	16	84			84	
0^+			12.15	0.001	1	99	3	96		
4^+			12.14	0.007	1	99		99		
2^+			12.12	0.008	1	99		98		
0^+	16.62	0.717	17.21	0.633	88	12	10	0.5		
0^+			11.28	0.092	12	88	85	2		
1^-	11.19	0.720	10.90	0.680	94.1	5.9				5.8
3^-	9.50	0.762	9.23	0.735	95.9	4.1			4.0	

Table 2. Excitation energy and total spectral strengths obtained for the principal solutions of DRPA and two-phonon ERPA equations, including the total contributions of ph and two-phonon configurations to the ERPA solutions. The individual contributions of the relevant two-phonon states are also indicated.

5. Conclusions

Self-consistent Green's function theory has been applied to study 2h1p correlations at small missing energies for the nucleus of ^{16}O. The method of the Faddeev equations allows to treat the coupling of ph and pp(hh) collective modes to the sp motion, The effects of fragmentation have been included through the dressing of the sp propagator. This approach allows to identify the important role played by the low-lying excited states of ^{16}O. These are essential to generate many of the fragments with small spectroscopic factors that are seen experimentally, examples of which are the $d_{5/2}$ and $p_{3/2}$ states of ^{15}N at 5.20 MeV and $\sim$9 MeV.

The main impediment in obtaining a good theoretical description of the single particle spectral function of ^{16}O has been identified in the poor description of the excitation spectrum, as obtained by solving the standard (D)RPA equations. We have improved on this by computing the effects of mixing of ph states with two-phonon configurations. The results show that these contributions explain the formation of several excited states observed at low energy which are not obtained by RPA calculations. However, it appears that a full solution of the spectrum of ^{16}O with this method requires to consider up to four-phonon states and the interaction in the pp and hh channels [31].

Acknowledgments

This work was supported in part by the Natural Sciences and Engineering Research Council of Canada (NSERC) and in part by the U.S. National Science Foundation

under Grants No. PHY-9900713 and PHY-0140316.

References

[1] S. C. Pieper and R. B. Wiringa, Ann. Rev. Nucl. Part. Sci. **51**, 53 (2001).

[2] P. Navrátil and B. R. Barrett, Phys. Rev. C **57**, 3119-3128 (1998); P. Navrátil and W. E. Ormand, Phys. Rev. C **68**, 034305 (2003).

[3] K. Kovalski *et al.*, Phys. Rev. Lett. **92**, 132501 (2004). D. J. Dean *et al.*, Phys. Rev. C **69**, 054320 (2004).

[4] R. Id Betan *et al.*, Phys. Rev. Lett. **89**, 042501 (2004). N. Michel *et al.*, Phys. Rev. Lett. **89**, 042502 (2004); Phys. Rev. C **67**, 054311 (2003).

[5] V. R. Pandharipande, I. Sick and P. de Witt Huberts, Rev. Mod.. Phys. **69**, 981 (1997).

[6] W. H. Dickhoff and C. Barbieri, Prog. Part. Nucl. Phys. **52**, 377 (2004).

[7] L. Lapikás, Nucl. Phys. **A553**, 297c (1993);

[8] M. Leuschner *et al.*, Phys. Rev. C **49**, 955 (1994).

[9] M. F. van Batenburg, Ph. D. Thesis, University of Utrecht, 2001.

[10] M. Radici, W. H. Dickhoff, and E. R. Stoddard, Phys. Rev. C **66**, 014613 (2002).

[11] S. Boffi, C. Giusti, F. D. Pacati, and M. Radici, *Electromagnetic Response of Atomic Nuclei*, Oxford Studies in Nuclear Physics (Clarendon Press, Oxford, 1996).

[12] J. M. Udías, J. A. Caballero, E. Moya de Guerra, J. R. Vignote, and A. Escuderos, Phys. Rev. C **64**, 024614 (2001).

[13] L. Lapikás, J. Wesseling, and R. B. Wiringa Phys. Rev. Lett. **82**, 4404-4407 (1999).

[14] D. Rohe *et al.*, `nucl-ex/0405028`; To be published on Phys. Rev. Lett.

[15] K. Amir-Azimi-Nili, H. Müther, L. D. Skouras, and A. Polls, Nucl. Phys. **A604**, 245 (1996);

[16] W. J. W. Geurts, K. Allaart, W. H. Dickhoff, and H. Müther, Phys. Rev. C **53**, 2207 (1996).

[17] C. Barbieri and W. H. Dickhoff, Phys. Rev. C **65**, 064313 (2002).

[18] C. Barbieri and W. H. Dickhoff, Phys. Rev. C **68**, 014311 (2003).

[19] C. Barbieri and W. H. Dickhoff, Phys. Rev. C **63**, 034313 (2001).

[20] A. L. Fetter and J. D. Walecka, *Quantum Theory of Many-Particle Physics* (McGraw-Hill, New York, 1971).

[21] A. A. Abrikosov, L. P. Gorkov and I. E. Dzyaloshinski, *Methods of Quantum Field Theory in Statistical Physics* (Dover, New York, 1975).

[22] G. Baym and L. P. Kadanoff, Phys. Rev. **124**, 287 (1961).

[23] P. Ring and P. Schuck, *The Nuclear Many-body Problem* (Springer, New York, 1980).

[24] W. J. W. Geurts, K. Allaart, and W. H. Dickhoff, Phys. Rev. C **50**, 514 (1994).

[25] W. Glöckle, *The Quantum Mechanical Few-Body Problem* (Springer, Berlin, 1983).

[26] H. Müther and P. Sauer, in *Computational Nuclear Physics* ed. by K.-H. Langanke *et al.* (Springer Berlin, 1993).

[27] R. Machleidt, Adv. Nucl. Phys. **19**, 191 (1989).

[28] D. Van Neck, M.Waroquier, A. E. L. Dieperink, S C. Pieper, and V. R. Pandharipande, Phys. Rev. C **57**, 2308 (1998).

[29] J. Yuan, Ph.D. thesis, Washington University, St. Louis, 1994.

[30] C. Barbieri and B. K. Jennings, `nucl-th/0408017`; To be published on Nucl. Phys. A.

[31] H. Feshbach and F. Iachello, Phys. Lett. **B45**, 7 (1973); Ann. Phys. **84**, 211 (1974).

[32] W. H. Dickhoff, in *Condensed Matter Theories. Vol. 3*, ed. J. S. Arponen, R. F. Bishop and M. Manninen (Plenum, New York 1988) p. 261.

[33] G. E. Brown, and A. M. Green, Nucl. Phys. **75**, 401 (1966); E. K. Warburton, B. A. Brown, and D. J. Millener, Phys. Lett. **B293**, 7 (1992).

[34] T. N. Buti *et al.*, Phys. Rev. C **33**, 755 (1986).